

Glasslike thermal conductivity and narrow insulating gap of EuTiO_3

Alexandre Jaoui^{1,2,*}, Shan Jiang^{2,*}, Xiaokang Li^{2,‡}, Yasuhide Tomioka³, Isao H. Inoue³, Johannes Engelmayr⁴, Rohit Sharma⁴, Lara Pätzold⁴, Thomas Lorenz⁴, Benoît Fauqué¹ and Kamran Behnia²

¹JEIP, USR 3573 CNRS, Collège de France, PSL Research University, 11, Place Marcelin Berthelot, 75231 Paris Cedex 05, France

²Laboratoire de Physique et d'Étude des Matériaux (ESPCI - CNRS - Sorbonne Université), PSL Research University, 75005 Paris, France

³National Institute of Advanced Industrial Science and Technology (AIST), Tsukuba 305-8565, Japan

⁴II. Physikalisches Institut, Universität zu Köln, 50937 Köln, Germany



(Received 27 June 2023; accepted 25 August 2023; published 28 September 2023)

Crystals and glasses differ by the amplitude and the temperature dependence of their thermal conductivity. However, there are crystals known to display glasslike thermal conductivity. Here, we show that EuTiO_3 , a quantum paraelectric known to order antiferromagnetically at 5.5 K, is one such system. The temperature dependence of resistivity and Seebeck coefficient yield an insulating band gap of ~ 0.22 eV. Thermal conductivity is drastically reduced. Its amplitude and temperature dependence are akin to what is seen in amorphous silica. Comparison with nonmagnetic perovskite solids, SrTiO_3 , KTaO_3 , and EuCoO_3 , shows that what impedes heat transport are $4f$ spins at Eu^{2+} sites, which couple to phonons well above the ordering temperature. Thus, in this case, superexchange and valence fluctuations, not magnetic frustration, are the drivers of the glasslike thermal conductivity.

DOI: [10.1103/PhysRevMaterials.7.094604](https://doi.org/10.1103/PhysRevMaterials.7.094604)

I. INTRODUCTION

In most insulating crystals, the flow of heat can be understood by considering the response of a gas of phonons to a temperature gradient. This picture, first drawn by Peierls [1], using a linearized Boltzmann equation, is remarkably successful in describing the thermal conductivity, κ , of most insulators [2,3]. It explains why at an intermediate temperature, κ peaks [4], separating a high-temperature decrease by warming (due to anharmonicity), and a low-temperature decrease by cooling (due to phonon depopulation). In amorphous solids, on the other hand, there is no such peak in $\kappa(T)$ and heat diffuses thanks to off-diagonal coupling across harmonic branches [5–8].

Some crystals, however, display glasslike thermal conductivity [9–15]. The thermal conductivity of these materials can be very low and/or feature a monotonic temperature dependence (lacking the T^{-1} decrease at high temperature). They are sought after, since a low lattice thermal conductivity would lead to a large thermoelectric figure of merit [16].

EuTiO_3 (ETO) is a perovskite with a cubic structure at room temperature [17]. Its electric permittivity increases upon cooling without giving rise to a ferroelectric instability. This quantum paraelectric behavior [18] is akin to what has been

seen in other ABO_3 compounds such as SrTiO_3 (STO) and KTaO_3 (KTO). In contrast to them, however, it magnetically orders at $T_N = 5.5$ K, with an antiferromagnetic alignment of the nearest neighbor Eu^{2+} spins [19,20]. Like STO, but at higher temperatures, it also goes through an antiferrodistortive (AFD) transition where adjacent TiO_6 octahedra rotate in opposite directions [21]. Upon doping, either with oxygen vacancies [22] or La substitution of Ti [23], it becomes a dilute metal [22–24], but without a superconducting ground state.

Here, we show that the temperature dependence of thermal conductivity in ETO is glasslike and its amplitude, over a broad temperature range starting from room temperature and extending to cryogenic temperatures, is lower than in STO and KTO. The drastic attenuation of thermal conductivity occurs well above the Néel temperature and when the magnetic entropy is saturated to its expected value. This points to an unusual version of spin-phonon coupling such as the phonon-paramagnon hybridization postulated by Bussmann-Holder *et al.* [17].

Evidence for spin-lattice coupling in ETO has been around for more than two decades [20]. However, it was restricted to temperatures comparable to the magnetic ordering. According to our findings, the phonon mean free path is affected by spins at Eu sites even at high temperature when there is neither a magnetic order nor a field-dependent entropy.

Monitoring the temperature dependence of electrical conductivity and thermopower in insulating EuTiO_3 , we find an activation gap of 0.11 eV, indicating that the intrinsic transport band gap in EuTiO_3 is as low as ~ 0.2 eV, much smaller than the gaps found by optical studies, but close to what is expected by *ab initio* calculations [25,26].

The narrow gap between the chemical potential and Eu^{2+} energy level and the random orientation of large magnetic

*These authors contributed equally to this paper.

†Present address: Fakultät für Physik, Ludwig-Maximilians Universität München, Geschwister-Scholl-Platz 1, 80539 München, Germany.

‡Present address: Wuhan National High Magnetic Field Center and School of Physics, Huazhong University of Science and Technology, Wuhan 430074, China.

moments in the paramagnetic state emerge as principal suspects shortening the lifetime of heat carrying phonons at elevated temperatures in the paramagnetic state.

In contrast to many other crystals displaying glasslike conductivity, ETO is not a spin liquid candidate, but a simple G -type antiferromagnet and there is no magnetic frustration. In this context, the glassy behavior could be framed in a picture of off-diagonal coupling across harmonic modes [7,15], which in this case would be phonons and paramagnons.

II. RESULTS

A. Activation and band gap

Figure 1(a) shows the temperature dependence of electrical resistivity ρ in as-grown EuTiO₃ (ETO) single crystals. One can see that ρ increases by seven orders of magnitude upon cooling from 360 K to 50 K.

An Arrhenius activation behavior becomes visible by plotting $\ln\rho$ as a function of the inverse of temperature [Fig. 1(b)]. The activation gap Δ is ~ 0.11 eV. The Hall resistivity (see the Supplemental Material [27]) also shows an Arrhenius behavior with a comparable Δ . At low temperature, resistivity begins to saturate when the Hall carrier density is as low as 10^{10} cm⁻³ (see the Supplemental Material [27]). This implies an extremely low level of extrinsic donors. An activated behavior in longitudinal and Hall resistivities of as-grown ETO crystals was previously reported by Engelmayer *et al.* [22], whose study focused on the emergence of metallicity in oxygen-deficient ETO.

This activated behavior is also confirmed by our measurements of the Seebeck coefficient [see Fig. 1(c)] and the temperature dependence of the electric permittivity [22].

The thermoelectric power has a negative sign and an amplitude in the range of mV/K, typical of a narrow gap semiconductor. The Seebeck coefficient in an intrinsic semiconductor is expected to be $\approx \frac{k_B}{e} \frac{\Delta}{k_B T}$ [28]. Thus, by plotting S as a function of T^{-1} (see the inset), one expects to see a straight line whose slope yields Δ . As seen in the inset of Fig. 1(c), this is indeed what our data yields, with $\Delta \approx 0.1$ eV. Note that this temperature dependence is qualitatively distinct from what is expected in extrinsic semiconductors [29] as seen, for example, in the case of Nb-doped STO [30].

Thus, the temperature dependence of the electric conductivity and the Seebeck coefficient both point to a similar energy gap between the chemical potential and the conduction band. The Hall and the Seebeck coefficients are both negative, indicating that carriers are electronlike and thermally excited to live in the conduction band originating from Ti- d orbitals.

Both ρ and S show an anomaly near 260 K, which we identify as the temperature of the structural transition in ETO [17,31]. Like STO [32], this transition makes ETO tetragonal [33]. We cannot rule out a very small difference in the amplitude of the activation gap between the cubic and the tetragonal phases [see the inset of Fig. 1(b)]. We also detected an unexpected and reproducible hysteresis near this phase transition. Taken at its face value, this indicates that this structural phase transition is first order (see the Supplemental Material).

Assuming that the chemical potential is halfway between the valence and conduction bands leads us to conclude that

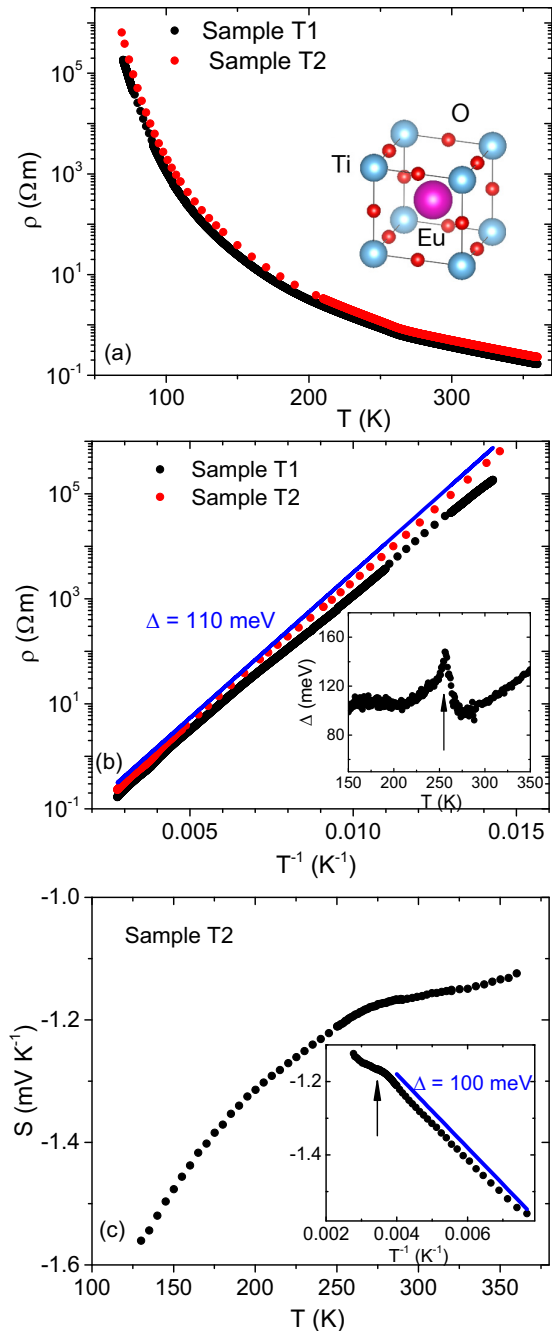


FIG. 1. Electrical resistivity, thermopower and activation gap of EuTiO₃. (a) Resistivity, ρ , as a function of temperature in two single crystals of EuTiO₃ in a semilogarithmic plot. The inset shows the unit cell (in the cubic phase). (b) Arrhenius plot of the same data: $\ln\rho$ vs T^{-1} . The solid blue line corresponds to $\Delta = 0.11$. The inset shows the temperature variation of $\Delta = -k_B T^2 \frac{\partial \ln \rho}{\partial T}$, with an arrow pointing to T_{AFD} , the temperature of antiferrodistortive transition. (c) Seebeck coefficient, S as a function of temperature. The data is restricted to $T > 120$ K, below which measurement becomes problematic. The inset shows S as a function of T^{-1} . The solid blue lines correspond to $\Delta = 0.1$ eV. The arrow points to T_{AFD} .

the band gap of ETO is ≈ 0.22 eV. This is remarkably smaller than the 3.2 eV gap of STO [34], but only slightly smaller than what a recent DFT calculation [26] found (0.27–0.33 eV). According to another and earlier theoretical study [25], the

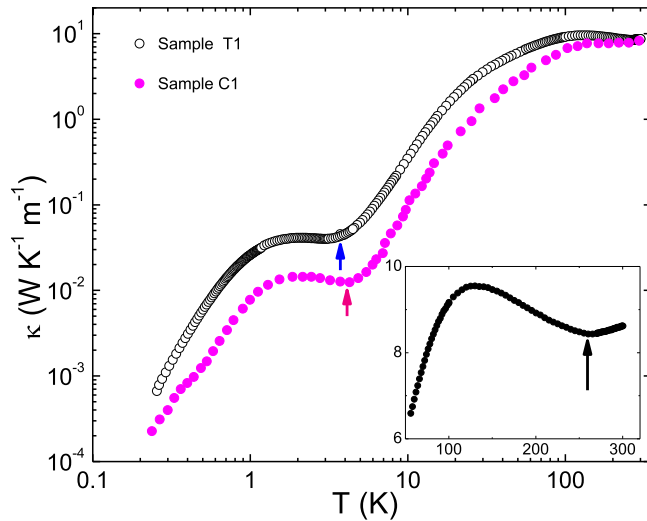


FIG. 2. Thermal conductivity of two EuTiO_3 crystals. Thermal conductivity, κ , as a function of temperature in two EuTiO_3 crystals in a log-log plot. The arrow points to a minimum near the Néel temperature. The inset shows a linear plot, with an arrow pointing to T_{AFD} .

magnitude of the band gap in ETO depends on the amplitude of the Hubbard repulsion energy (U). A realistic U (5–6 eV) would lead to a band gap of 0.2–0.4 eV. Thus, the narrow gap detected by our transport studies is close to what is intrinsically expected in this solid. Optical probes, however, have detected a larger gap (0.8–0.9 eV) [35,36]. Such larger energy scales are possible indications that the density of states (DOS) near the $\text{Eu-}f$ level is not featureless [26].

Let us keep in mind the contrast between ETO on one hand, and STO and KTO on the other hand. The first has a valence band originating from $\text{Eu-}f$ orbitals close to the chemical potential, while the two others have a valence band emanating from $\text{O-}p$ orbitals and much further away from the chemical potential.

B. Thermal conductivity

Figure 2 shows the temperature dependence of thermal conductivity, κ , of two ETO crystals from slightly above room temperature down to dilution refrigerator temperatures. We measured several crystals and found that the thermal conductivity of all lies somewhere between the two cases shown in this figure. Moreover, we could not detect a correlation between the amplitude of κ and a weak variation of the saturation magnetization observed across various ETO samples (see the Supplemental Material [27]).

In contrast to typical crystalline insulators [4], κ does not show a prominent peak. As seen in the inset, there is a clear anomaly at T_{AFD} , and below this temperature κ rises by ten percent increase with cooling. However, there is no sign of a kinetic regime with $\kappa \propto T^{-1}$, as seen in many other insulators [37,38].

C. Crystals, glasses, and glasslike crystals

In order to put our observation in a proper context, we compare our data with what has been reported in the case

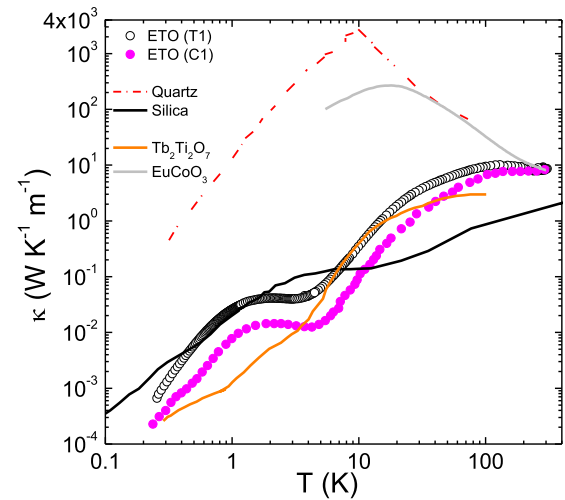


FIG. 3. Comparison with crystals, glasses, and glasslike crystals. Thermal conductivity as a function of temperature in crystalline quartz, in vitreous silica [39], in EuTiO_3 , and in the frustrated magnet $\text{Tb}_2\text{Ti}_2\text{O}_7$ [11]. The latter two crystalline compounds conduct heat like a glass rather than like a crystal. Also shown is the crystallike thermal conductivity of nonmagnetic EuCoO_3 [43].

of SiO_2 , which shows a spectacular difference in the thermal conductivity in its crystalline and amorphous structures [39]. As seen in Fig. 3, κ in amorphous silica monotonically decreases with cooling, in contrast to crystalline quartz, which has a prominent peak. At any given temperature, the crystal conducts heat at least an order of magnitude more than the glass [4]. Not only the thermal conductivity of ETO is similar to silica in temperature dependence, but also in the cryogenic temperature range surrounding the Néel temperature ($T_N \simeq 5.5$ K), the ETO crystalline samples conduct heat less than amorphous silica. The order of magnitude of thermal conductivity and its temperature dependence in ETO is comparable with other crystalline solids displaying a glasslike thermal conductivity, such as $\text{Tb}_2\text{Ti}_2\text{O}_7$ [11], $\text{Tb}_3\text{Ga}_5\text{O}_{12}$ [40], $\text{Na}_4\text{Ir}_3\text{O}_8$ [41], $\text{Pr}_2\text{Ir}_2\text{O}_7$ [42], and $\text{La}_{0.2}\text{Nd}_{0.4}\text{Pb}_{0.4}\text{MnO}_3$ [9]. In order to allow a direct comparison, Fig. 3 includes the data for $\text{Tb}_2\text{Ti}_2\text{O}_7$ [11], the compound with the lowest thermal conductivity among these frustrated magnets. Note that in contrast to other members of this club of materials, EuTiO_3 is a G -type antiferromagnet and is not frustrated.

As a further comparison, we also include κ of EuCoO_3 [43], which displays a temperature dependence typical of a crystalline insulator. EuCoO_3 is a perovskite like ETO, but it has an orthorhombic symmetry, and the valence is Eu^{3+} with only six electrons in the $4f$ shell. According to Hund's rules, this causes a vanishing magnetic moment ($J = L - S = 0$), in agreement with the experimentally observed van Vleck susceptibility [44], drastically different from the large local moments of $7 \mu_B/\text{Eu}^{2+}$ in ETO.

D. ETO compared to its nonmagnetic sisters

Figure 4 compares the thermal conductivity of ETO and two other ABO_3 perovskites. SrTiO_3 (STO) and KTaO_3 (KTO) are also quantum paraelectric, but not magnetic solids. Our new data on these two materials is in good agreement with

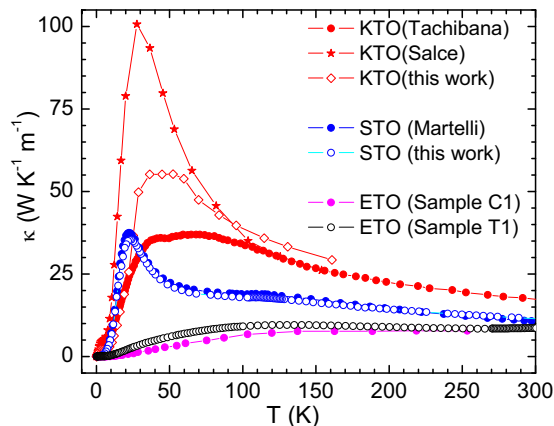


FIG. 4. Thermal conductivity of three quantum paraelectric solids. Thermal conductivity of the two EuTiO_3 samples in a linear scale compared with thermal conductivity of SrTiO_3 [45] and KTaO_3 [12,46]. Note the drastic reduction of thermal conductivity in the paramagnetic EuTiO_3 . The visible sample dependence of the data for each material is much smaller than the difference between the three compounds.

previous studies of heat transport in STO [45,47,48] and in KTO [46–48]. In both cases, there is also a visible sample dependence, which is more pronounced near the peak. However, this sample dependence is much smaller than the difference between the three compounds. At room temperature, this difference is small, yet visible: $\kappa(300 \text{ K})$ is $\approx 9 \text{ W}/(\text{K m})$ in ETO, $\approx 11 \text{ W}/(\text{K m})$ in STO, and $\approx 17 \text{ W}/(\text{K m})$ in KTO. Much more drastic is the difference in the temperature dependence between the three sister compounds. The enhancement with cooling observed in the other perovskites is absent in ETO. This difference extends over the full temperature range above the magnetic ordering. The difference is somewhat attenuated below the ordering temperature. Above the ordering temperature (say, at 10 K) the thermal conductivity of STO is 50 times larger than the thermal conductivity of ETO. Below the Néel temperature (say, at 1 K), the difference between the two is only a factor of two.

It is instructive to scrutinize the specific heat of the three sister compounds. Figure 5(a) shows that C/T of STO, ETO, and KTO approach each other toward room temperature and reach $C \approx 100 \text{ J}/(\text{mol K})$. With five atoms, one expects the specific heat saturating to the Dulong-Petit value of $5 \times 3N_A k_B = 124.6 \text{ J}/(\text{mol K})$. Here, N_A is the Avogadro number and k_B the Boltzmann number. The specific heat of STO, heated to 1800 K approaches this value [49]. This is a remarkably high temperature, broadly compatible but twice larger than the highest energy scale in the phonon spectrum of these solids ($\approx 100 \text{ meV}$) [31,50]. A systematic difference in the specific heat evolves at lower temperatures. As seen in the inset of Fig. 5(a), all three solids show a peak in the temperature dependence of $\frac{C}{T^3}$. In the case of STO, this peak is known to be caused by the presence of Einstein modes [51,52]. Similar peaks are visible for KTO and for ETO, and the position of this peak shifts with the increase in the molar mass. In STO (184 g/mol), it occurs at 30 K, in ETO (248 g/mol) at 25 K, and in KTO (267 g/mol) at 12 K. In the case of ETO, a distinct additional contribution shoots up below 15 K, which

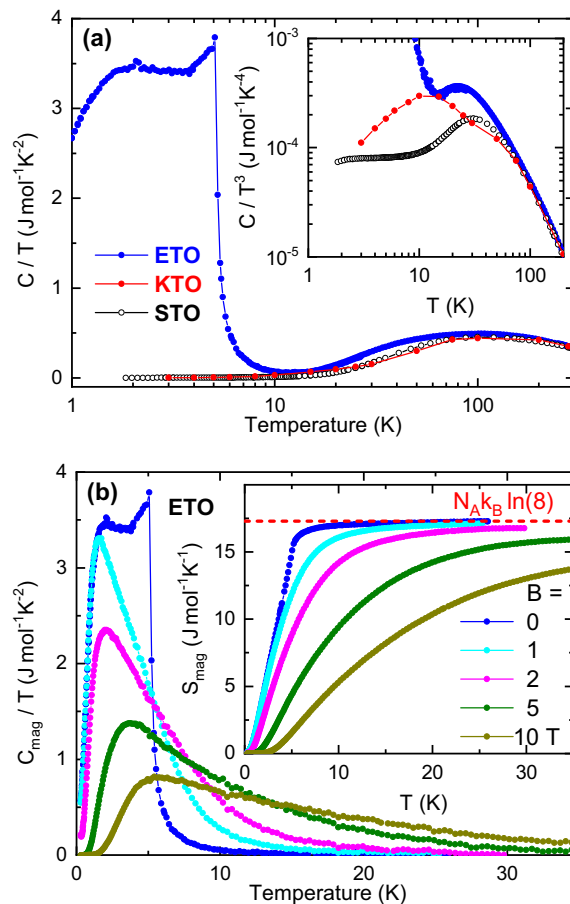


FIG. 5. Specific heat in three quantum paraelectric solids. (a) Temperature dependence of the total specific heat in KTaO_3 , SrTiO_3 , and EuTiO_3 plotted as C/T vs T . The inset is an enlarged view of the same data shown as $\frac{C}{T^3}$ vs T . Note the presence of Einstein modes in all three solids and the additional magnetic specific heat in ETO emerging below 15 K. (b) Evolution of C_{mag}/T of ETO for different magnetic fields up to 10 T. The inset shows the corresponding magnetic entropy $S_{\text{mag}} = \int C_{\text{mag}}/T dT$ of ETO and the maximum magnetic entropy $N_A k_B \ln(2S + 1)$ of a spin 7/2 system is indicated by the dashed line.

signals strong magnetic fluctuations above the Néel ordering temperature of the Eu^{2+} spins.

E. Field dependence

As reported previously [53], the specific heat in ETO displays a strong dependence on magnetic field. In order to separate the magnetic C_{mag} and the phononic C_{phon} contribution, we subtracted from the total specific heat of EuTiO_3 the measured specific heat of SrTiO_3 (with a temperature rescaled by a factor of 0.83 such that the positions of the C/T^3 maxima of both materials match). Note that this scaling factor is close to the ratio of the molar masses $\sqrt{M_{\text{STO}}/M_{\text{ETO}}} = 0.86$, the expected ratio of their Debye temperatures. Figure 5(b) shows the magnetic heat capacity C_{mag}/T of EuTiO_3 for different magnetic fields from 0 up to 10 T applied along a $[100]_c$ direction of the cubic room temperature phase. The sharp zero-field anomaly signals the antiferromagnetic order at $T_N = 5.5 \text{ K}$

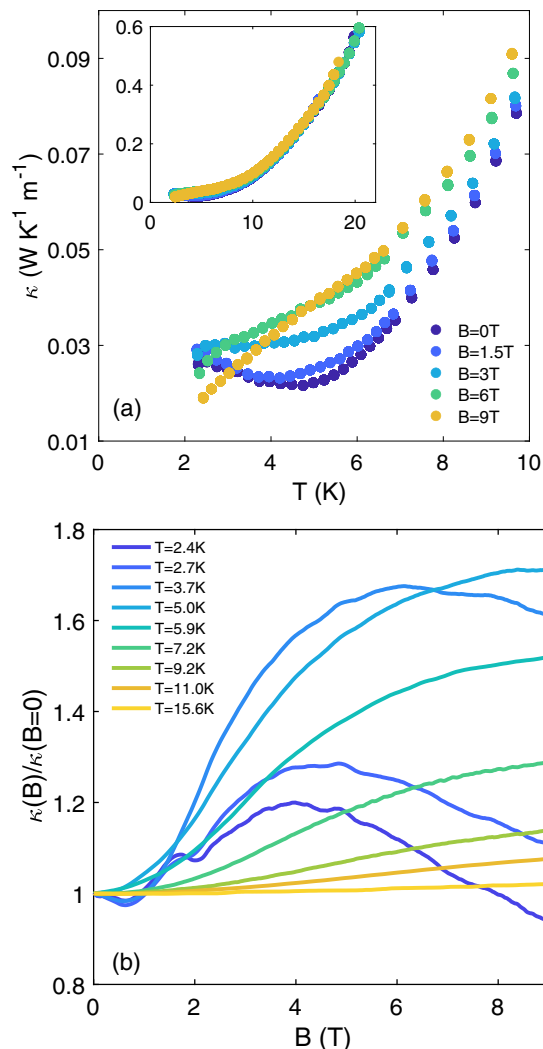


FIG. 6. Field dependence of thermal conductivity in EuTiO_3 . (a) κ vs. T from 2 K to 10 K for $B = 0$ T to 9 T. (b) Normalized κ vs B for $T = 2.4$ K to 15.6 K for $B//[001]$.

that gets strongly broadened already in a field of 1 T. This reflects the magnetic-field-induced switching to the polarized magnetic state, which sets in around 1.2 T in ETO (see, e.g., the Supplemental Material [27] or [54]) and, consequently, the C_{mag}/T data in larger fields no longer signal a spontaneous magnetic ordering transition, but a continuous evolution of magnetic entropy as it is the case for ferromagnets in an external magnetic field. In fact, the C_{mag}/T data of EuTiO_3 strongly resembles the corresponding data obtained on the Eu^{2+} -based ferromagnet EuC_2 , which orders at $T_C = 14$ K [55]. The magnetic entropy obtained by integrating C_{mag}/T is displayed in the inset of Fig. 5(b) and reveals that the full magnetic entropy $N_A k_B \ln(2S + 1)$ of a spin $7/2$ system is reached above about 15 K for zero field and also for 1 T, whereas for fields above 2 T the entropy evolution drastically broadens and extends to much higher temperatures.

The field dependence of κ , shown in Fig. 6, further points to an intricate coupling between Eu^{2+} spins and heat-carrying phonons. Thermal conductivity begins to depend on magnetic field below 15 K. Interestingly, as seen in the inset of Fig. 5,

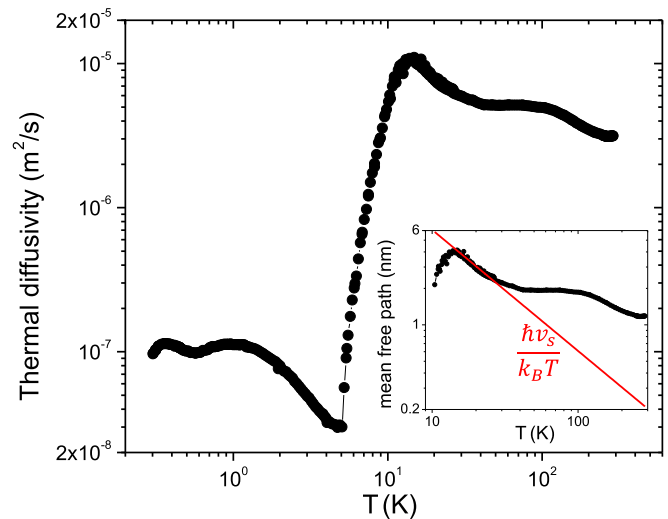


FIG. 7. Thermal diffusivity of EuTiO_3 and the mean free path of phonons. Temperature dependence of thermal diffusivity, D , by taking the ratio of thermal conductivity and the specific heat per volume in sample C1. Note the drastic drop across the magnetic transition. The inset shows the temperature dependence of the mean free path in the paramagnetic phase, assuming that all phonons have the same scattering time and velocity for the same sample. The red solid line represents the inverse of the wavevector of the thermally excited acoustic phonons.

this is the temperature below which there is a significant magnetic entropy.

Above T_N , magnetic field slightly amplifies κ , indicating a weakening of the spin-induced localization of phonons. This field-induced amplification of κ in ETO is modest, in contrast to the thirtyfold field-induced amplification of the ultralow thermal conductivity in $\text{Tb}_2\text{Ti}_2\text{O}_7$ [11].

Below 3 K, well below the Néel temperature, the field dependence becomes nonmonotonic (see Fig. 6). We leave the quantitative understanding of the field dependence of κ in EuTiO_3 as a subject of study for future investigations.

F. Thermal diffusivity of EuTiO_3 and the mean free path of phonons

Replacing Sr by Eu reduces the thermal conductivity in a wide temperature range and enhances the specific heat below 15 K. Therefore, the ratio of thermal conductivity [in $\text{W}/(\text{K m})$] to specific heat per volume [in $\text{J}/(\text{K m}^3)$], i.e., the thermal diffusivity, D , (in m^2/s) is drastically modified. It is plotted in Fig. 7. The most striking feature of $D(T)$ is its two-orders-of-magnitude drop at the Néel temperature. Within the entry to the antiferromagnetically ordered phase, at 5.5 K, it becomes exceptionally low. Its minimum, $0.03 \text{ mm}^2/\text{s}$, is almost two orders of magnitude lower than the thermal diffusivity of a typical glass [56]. Note that this is not the thermal diffusivity of phonons, but of the whole solid. Its low amplitude, which is a consequence of the combination of an unusually low lattice thermal conductivity and a very large magnetic entropy, may find applications in heat management in a cryogenic context.

The thermal conductivity of an insulator can be written as

$$\kappa = \sum_{s,\mathbf{q}} C_s(\mathbf{q})v_s^2(\mathbf{q})\tau_s(\mathbf{q}). \quad (1)$$

The index s refers to different modes and \mathbf{q} is the wave vector. C_s , v_s , and τ_s are specific heat, velocity, and scattering time. There are modes contributing to the total specific heat ($C = \sum_s C_s$), but not to thermal conductivity, because of their negligible velocity. Theoretically [17], paramagnons in the paramagnetic state have no dispersion and therefore do not carry heat. They can, however, reduce the phonon thermal transport. In ETO, phonons not only dominate thermal conductivity, but also, at least down to 15 K, the specific heat. Therefore, one can simply write $\kappa = 1/3Cv_s\ell_{ph}$. This neglects the q dependence of the scattering time and assumes that all modes have the same velocity. Taking $v_s = 6.8$ km/s, the measured sound velocity in STO [57], and in reasonable agreement with the dispersion of acoustic branches in ETO [31], one can estimate ℓ_{ph} , shown in the inset of Fig. 7. Comparing it to the inverse of the wave vector of thermally excited phonons $q_s = \frac{k_B T}{\hbar v_s}$, one finds that below 20 K, $q_s \ell_{ph} \cong 1$, reminiscent of the Anderson localization. There is a drop at 15 K, below which specific heat is no more phonon dominated.

III. DISCUSSION

Evidence for a coupling between spin and lattice degrees of freedom in this compound was first reported by Katsufuji and Takagi [20], who found that when the spins order at 5.5 K, the electric permittivity of ETO drops by seven percent and this drop is suppressed by the application of a magnetic field of the order of 3 T. This magnetoelectric effect implies coupling between Eu^{2+} spins and the soft mode governing the electric permittivity. Reuvekamp *et al.* [58] have found a quantitative agreement between the amplitude of the magnetoelectric effect and the low-temperature magnetostriction of the system.

Our main finding is that lattice-spin coupling drastically attenuates the propagation of heat in ETO, even at temperatures where magnetic ordering is absent and magnetic entropy is practically saturated at its maximum value $k_B \ln(2S + 1)/\text{spin}$. This implies that even when the spins are randomly oriented, heat-carrying phonons couple to Eu^{2+} states and their large magnetic moments (6.9–7 μ_B). According to Ref. [26], without incorporating the loss of spin symmetry, the DFT calculations cannot explain the absence of metallicity and the finite band gap of the paramagnetic phase.

The random orientation of magnetic moments at Eu sites (see Fig. 8) is the most plausible source of phonon localization. The superexchange interaction between Eu spins occurs through Ti ions [59]. The interatomic force constant can depend on the relative orientation of spins. The calculated phonon frequencies for parallel or antiparallel alignment of adjacent spins are not the same [60], which implies that phonons cannot keep a well-defined dispersion in the presence of random spin orientation.

The narrow energy separation between the Eu^{2+} energy level and the chemical potential may also play a role. In some Eu-based metals, the thermoelectric response has been linked to the temperature dependence of Eu valence [61]. Remarkably, a theoretical study [62] has concluded that the

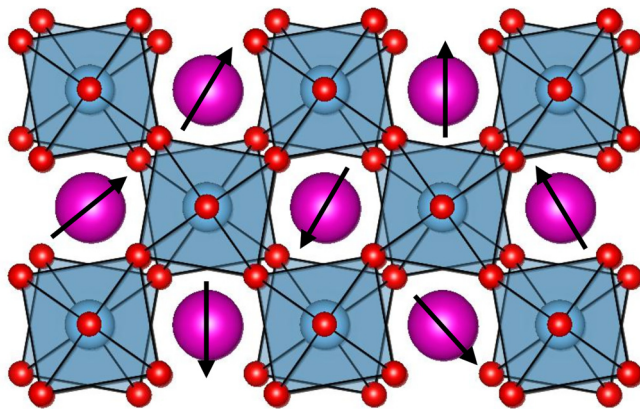


FIG. 8. Crystal structure of EuTiO_3 in its paramagnetic phase. Random magnetic moments at Eu sites are located between TiO_6 octahedra, which are tilted off each other. Superexchange interaction between these spins involves Ti and oxygen atoms. This can impede phonons to have a well-defined wave-vector over long distances.

contribution of optical phonons to the overall lattice thermal conductivity is unusually large in this lattice structure. The energy of the highest optical phonon in this crystal structure [63] and the distance between the Eu f level and the chemical potential are both ≈ 0.1 eV. This may facilitate coupling between optical phonons and Eu valence fluctuations.

Inelastic neutron scattering is a promising probe of this physics. In the case of $\text{Tb}_3\text{Ga}_5\text{O}_{12}$, for example, it documented the coupling between spin and lattice [64]). A recent study on STO [65] has found evidence for an unusual hybridization between acoustic and optic phonon branches. No neutron scattering data is presently available to compare ETO with STO.

Finally, let us note that the glasslike thermal conductivity of EuTiO_3 , in contrast to spin-liquid crystals, occurs in a solid with a simple G -type antiferromagnetic ground state [19]. A formal theoretical treatment may be achieved by complementing the picture drawn by Eq. (1) with an “off-diagonal” coupling between different vibrational states [7,8,15]:

$$\kappa_{od} = \sum_{\substack{s \neq s' \\ ss', \mathbf{q}}} C_{ss'}(\mathbf{q})v_{ss'}^2(\mathbf{q})\tau_{ss'}(\mathbf{q}). \quad (2)$$

This equation was conceived for nonmagnetic crystals, in which harmonic coupling occurs across phonon branches [7,15]. It can be extended to magnetic modes.

ACKNOWLEDGMENTS

We thank Annette Bussman-Holder, Yo Machida, Igor Mazin, and Nicola Spaldin for stimulating discussions. This work was supported in France by the JEIP-Collège de France, and by the Agence Nationale de la Recherche (ANR-18-CE92-0020-01; ANR-19-CE30-0014-04), and a grant by the Ile de France regional council. In Germany, it was supported by the DFG (German Research Foundation) via Project No. LO 818/6-1. I.H.I. in Japan was supported by the Japan Society for the Promotion of Science (JSPS) KAKENHI Grant No. 18H03686 and the Japan Science and Technology Agency (JST) CREST Grant No. JPMJCR19K2.

- [1] R. Peierls, Zur kinetischen Theorie der Wärmeleitung in Kristallen, *Ann. Physik* **395**, 1055 (1929).
- [2] L. Lindsay, D. A. Broido, and T. L. Reinecke, *Ab initio* thermal transport in compound semiconductors, *Phys. Rev. B* **87**, 165201 (2013).
- [3] A. Subedi, First principles study of thermal conductivity of In_2O_3 in relation to Al_2O_3 , Ga_2O_3 , and KTaO_3 , [arXiv:2101.02664](https://arxiv.org/abs/2101.02664).
- [4] J. W. Vandersande and C. Wood, The thermal conductivity of insulators and semiconductors, *Contemp. Phys.* **27**, 117 (1986).
- [5] P. B. Allen, J. L. Feldman, J. Fabian, and F. Wooten, Diffusons, locons and propagons: Character of atomic vibrations in amorphous Si, *Philos. Mag.* **B 79**, 1715 (1999).
- [6] H. R. Seyf and A. Henry, A method for distinguishing between propagons, diffusons, and locons, *J. Appl. Phys.* **120**, 025101 (2016).
- [7] M. Simoncelli, N. Marzari, and F. Mauri, Unified theory of thermal transport in crystals and glasses, *Nat. Phys.* **15**, 809 (2019).
- [8] L. Isaeva, G. Barbalinardo, D. Donadio, and S. Baroni, Modeling heat transport in crystals and glasses from a unified lattice-dynamical approach, *Nat. Commun.* **10**, 3853 (2019).
- [9] D. W. Visser, A. P. Ramirez, and M. A. Subramanian, Thermal Conductivity of Manganite Perovskites: Colossal Magnetoresistance as a Lattice-Dynamics Transition, *Phys. Rev. Lett.* **78**, 3947 (1997).
- [10] K. Takahata, Y. Iguchi, D. Tanaka, T. Itoh, and I. Terasaki, Low thermal conductivity of the layered oxide $(\text{Na}, \text{Ca})\text{Co}_2\text{O}_4$: Another example of a phonon glass and an electron crystal, *Phys. Rev. B* **61**, 12551 (2000).
- [11] Q. J. Li, Z. Y. Zhao, C. Fan, F. B. Zhang, H. D. Zhou, X. Zhao, and X. F. Sun, Phonon-glass-like behavior of magnetic origin in single-crystal $\text{Tb}_2\text{Ti}_2\text{O}_7$, *Phys. Rev. B* **87**, 214408 (2013).
- [12] M. Tachibana, Thermal conductivity of pyrochlore $\text{R}_2\text{Ti}_2\text{O}_7$ ($\text{R} = \text{rare earth}$), *Solid State Commun.* **174**, 16 (2013).
- [13] K. Sugii, M. Shimozawa, D. Watanabe, Y. Suzuki, M. Halim, M. Kimata, Y. Matsumoto, S. Nakatsuji, and M. Yamashita, Thermal Hall Effect in a Phonon-Glass $\text{Ba}_3\text{CuSb}_2\text{O}_9$, *Phys. Rev. Lett.* **118**, 145902 (2017).
- [14] M. Dutta, S. Matteppanavar, M. V. D. Prasad, J. Pandey, A. Warankar, P. Mandal, A. Soni, U. V. Waghmare, and K. Biswas, Ultralow thermal conductivity in chain-like TlSe due to inherent TI^+ rattling, *J. Am. Chem. Soc.* **141**, 20293 (2019).
- [15] R. Hanus, J. George, M. Wood, A. Bonkowski, Y. Cheng, D. L. Abernathy, M. E. Manley, G. Hautier, G. J. Snyder, and R. P. Hermann, Uncovering design principles for amorphous-like heat conduction using two-channel lattice dynamics, *Mater. Today Phys.* **18**, 100344 (2021).
- [16] G. J. Snyder and E. S. Toberer, Complex thermoelectric materials, *Nat. Mater.* **7**, 105 (2008).
- [17] A. Bussmann-Holder, Z. Guguchia, J. Köhler, H. Keller, A. Shengelaya, and A. R. Bishop, Hybrid paramagnon phonon modes at elevated temperatures in EuTiO_3 , *New J. Phys.* **14**, 093013 (2012).
- [18] K. A. Müller and H. Burkard, SrTiO_3 : An intrinsic quantum paraelectric below 4 K, *Phys. Rev. B* **19**, 3593 (1979).
- [19] T. R. McGuire, M. W. Shafer, R. J. Joenk, H. A. Alperin, and S. J. Pickart, Magnetic structure of EuTiO_3 , *J. Appl. Phys.* **37**, 981 (1966).
- [20] T. Katsufuji and H. Takagi, Coupling between magnetism and dielectric properties in quantum paraelectric EuTiO_3 , *Phys. Rev. B* **64**, 054415 (2001).
- [21] A. Bussmann-Holder, J. Köhler, R. K. Kremer, and J. M. Law, Relation between structural instabilities in EuTiO_3 and SrTiO_3 , *Phys. Rev. B* **83**, 212102 (2011).
- [22] J. Engelmayr, X. Lin, C. P. Grams, R. German, T. Fröhlich, J. Hemberger, K. Behnia, and T. Lorenz, Charge transport in oxygen-deficient EuTiO_3 : The emerging picture of dilute metallicity in quantum-paraelectric perovskite oxides, *Phys. Rev. Mater.* **3**, 051401(R) (2019).
- [23] Y. Tomioka, T. Ito, and A. Sawa, Magnetotransport properties of $\text{Eu}_{1-x}\text{La}_x\text{TiO}_3$ ($0 \leq x \leq 0.07$) single crystals, *J. Phys. Soc. Jpn.* **87**, 094716 (2018).
- [24] K. Maruhashi, K. S. Takahashi, M. S. Bahramy, S. Shimizu, R. Kurihara, A. Miyake, M. Tokunaga, Y. Tokura, and M. Kawasaki, Anisotropic quantum transport through a single spin channel in the magnetic semiconductor EuTiO_3 , *Adv. Mater.* **32**, 1908315 (2020).
- [25] R. Ranjan, H. S. Nabi, and R. Pentcheva, Electronic structure and magnetism of EuTiO_3 : a first-principles study, *J. Phys.: Condens. Matter* **19**, 406217 (2007).
- [26] O. I. Malyi, X.-G. Zhao, A. Bussmann-Holder, and A. Zunger, Local positional and spin symmetry breaking as a source of magnetism and insulation in paramagnetic EuTiO_3 , *Phys. Rev. Mater.* **6**, 034604 (2022).
- [27] See Supplemental Material at <http://link.aps.org/supplemental/10.1103/PhysRevMaterials.7.094604> for information regarding crystal growth, experimental techniques, and additional data, which includes Refs. [17,19,22,23,36,53,54,61,66,67].
- [28] K. Behnia, *Fundamentals of Thermoelectricity* (Oxford University Press, Oxford, 2015).
- [29] V. A. Johnson and K. Lark-Horovitz, Theory of thermoelectric power in semiconductors with applications to germanium, *Phys. Rev.* **92**, 226 (1953).
- [30] C. Collignon, P. Bourges, B. Fauqué, and K. Behnia, Heavy Nondegenerate Electrons in Doped Strontium Titanate, *Phys. Rev. X* **10**, 031025 (2020).
- [31] K. Z. Rushchanskii, N. A. Spaldin, and M. Ležaić, First-principles prediction of oxygen octahedral rotations in perovskite-structure EuTiO_3 , *Phys. Rev. B* **85**, 104109 (2012).
- [32] F. W. Lytle, X-ray diffractometry of low-temperature phase transformations in strontium titanate, *J. Appl. Phys.* **35**, 2212 (1964).
- [33] B. J. Kennedy, G. Murphy, E. Reynolds, M. Avdeev, H. E. R. Brand, and T. Kolodiazhyi, Studies of the antiferrodistortive transition in EuTiO_3 , *J. Phys.: Condens. Matter* **26**, 495901 (2014).
- [34] C. Collignon, X. Lin, C. W. Rischau, B. Fauqué, and K. Behnia, Metallicity and superconductivity in doped strontium titanate, *Annu. Rev. Condens. Matter Phys.* **10**, 25 (2019).
- [35] J. H. Lee, X. Ke, N. J. Podraza, L. F. Kourkoutis, T. Heeg, M. Roeckerath, J. W. Freeland, C. J. Fennie, J. Schubert, D. A. Muller, P. Schiffer, and D. G. Schlom, Optical band gap and magnetic properties of unstrained EuTiO_3 films, *Appl. Phys. Lett.* **94**, 212509 (2009).
- [36] H. Akamatsu, K. Fujita, H. Hayashi, T. Kawamoto, Y. Kumagai, Y. Zong, K. Iwata, F. Oba, I. Tanaka, and K. Tanaka, Crystal and electronic structure and magnetic properties of divalent europium perovskite oxides EuMO_3 ($M = \text{Ti}, \text{Zr}, \text{and Hf}$):

- Experimental and first-principles approaches, *Inorg. Chem.* **51**, 4560 (2012).
- [37] R. Berman, *Thermal Conduction in Solids* (Oxford University Press, Oxford, 1976).
- [38] L. Xu, B. Fauqué, Z. Zhu, Z. Galazka, K. Irmscher, and K. Behnia, Thermal conductivity of bulk In_2O_3 single crystals, *Phys. Rev. Mater.* **5**, 014603 (2021).
- [39] R. C. Zeller and R. O. Pohl, Thermal conductivity and specific heat of noncrystalline solids, *Phys. Rev. B* **4**, 2029 (1971).
- [40] A. V. Inyushkin and A. N. Taldenkov, Low-temperature thermal conductivity of terbium-gallium garnet, *J. Exp. Theor. Phys.* **111**, 760 (2010).
- [41] B. Fauqué, X. Xu, A. F. Bangura, E. C. Hunter, A. Yamamoto, K. Behnia, A. Carrington, H. Takagi, N. E. Hussey, and R. S. Perry, Thermal conductivity across the metal-insulator transition in the single-crystalline hyperkagome antiferromagnet $\text{Na}_{3+x}\text{Ir}_3\text{O}_8$, *Phys. Rev. B* **91**, 075129 (2015).
- [42] T. Uehara, T. Ohtsuki, M. Udagawa, S. Nakatsuji, and Y. Machida, Phonon thermal Hall effect in a metallic spin ice, *Nat. Commun.* **13**, 4604 (2022).
- [43] K. Berggold, M. Kriener, P. Becker, M. Benomar, M. Reuther, C. Zobel, and T. Lorenz, Anomalous expansion and phonon damping due to the Co spin-state transition in RCoO_3 , *Phys. Rev. B* **78**, 134402 (2008).
- [44] J. Baier, S. Jodlauk, M. Kriener, A. Reichl, C. Zobel, H. Kierspel, A. Freimuth, and T. Lorenz, Spin-state transition and metal-insulator transition in $\text{La}_{1-x}\text{Eu}_x\text{CoO}_3$, *Phys. Rev. B* **71**, 014443 (2005).
- [45] V. Martelli, J. L. Jiménez, M. Continentino, E. Baggio-Saitovitch, and K. Behnia, Thermal Transport and Phonon Hydrodynamics in Strontium Titanate, *Phys. Rev. Lett.* **120**, 125901 (2018).
- [46] B. Salce, J. L. Gravi, and L. A. Boatner, Disorder and thermal transport in undoped KTaO_3 , *J. Phys.: Condens. Matter* **6**, 4077 (1994).
- [47] E. F. Steigmeier, Field effect on the cochran modes in SrTiO_3 and KTaO_3 , *Phys. Rev.* **168**, 523 (1968).
- [48] X. Li, B. Fauqué, Z. Zhu, and K. Behnia, Phonon Thermal Hall Effect in Strontium Titanate, *Phys. Rev. Lett.* **124**, 105901 (2020).
- [49] D. de Ligny and P. Richet, High-temperature heat capacity and thermal expansion of SrTiO_3 and SrZrO_3 perovskites, *Phys. Rev. B* **53**, 3013 (1996).
- [50] U. Aschauer and N. A. Spaldin, Competition and cooperation between antiferrodistortive and ferroelectric instabilities in the model perovskite SrTiO_3 , *J. Phys.: Condens. Matter* **26**, 122203 (2014).
- [51] G. Burns, Comment on the low temperature specific heat of ferroelectrics, antiferroelectrics, and related materials, *Solid State Commun.* **35**, 811 (1980).
- [52] E. McCalla, M. N. Gastiasoro, G. Cassuto, R. M. Fernandes, and C. Leighton, Low-temperature specific heat of doped SrTiO_3 : Doping dependence of the effective mass and Kadowaki-Woods scaling violation, *Phys. Rev. Mater.* **3**, 022001(R) (2019).
- [53] A. P. Petrović, Y. Kato, S. S. Sunku, T. Ito, P. Sengupta, L. Spalek, M. Shimuta, T. Katsufuji, C. D. Batista, S. S. Saxena, and C. Panagopoulos, Electric field modulation of the tetragonal domain orientation revealed in the magnetic ground state of quantum paraelectric EuTiO_3 , *Phys. Rev. B* **87**, 064103 (2013).
- [54] A. Midya, P. Mandal, K. Rubi, R. Chen, J.-S. Wang, R. Mahendiran, G. Lorusso, and M. Evangelisti, Large adiabatic temperature and magnetic entropy changes in EuTiO_3 , *Phys. Rev. B* **93**, 094422 (2016).
- [55] O. Heyer, P. Link, D. Wandner, U. Ruschewitz, and T. Lorenz, Thermodynamic properties and resistivity of the ferromagnetic semiconductor EuC_2 , *New J. Phys.* **13**, 113041 (2011).
- [56] G. Yang, A. D. Migone, and K. W. Johnson, Heat capacity and thermal diffusivity of a glass sample, *Phys. Rev. B* **45**, 157 (1992).
- [57] B. Okai and J. Yoshimoto, Pressure dependence of the structural phase transition temperature in SrTiO_3 and KMnF_3 , *J. Phys. Soc. Jpn.* **39**, 162 (1975).
- [58] P. Reuvekamp, K. Caslin, Z. Guguchia, H. Keller, R. K. Kremer, A. Simon, J. Köhler, and A. Bussmann-Holder, Tiny cause with huge impact: polar instability through strong magneto-electric-elastic coupling in bulk EuTiO_3 , *J. Phys.: Condens. Matter* **27**, 262201 (2015).
- [59] H. Akamatsu, Y. Kumagai, F. Oba, K. Fujita, H. Murakami, K. Tanaka, and I. Tanaka, Antiferromagnetic superexchange via $3d$ states of titanium in EuTiO_3 as seen from hybrid hartree-fock density functional calculations, *Phys. Rev. B* **83**, 214421 (2011).
- [60] C. J. Fennie and K. M. Rabe, Magnetic and electric phase control in epitaxial EuTiO_3 from first principles, *Phys. Rev. Lett.* **97**, 267602 (2006).
- [61] U. Stockert, S. Seiro, N. Caroca-Canales, E. Hassinger, and C. Geibel, Valence effect on the thermopower of Eu systems, *Phys. Rev. B* **101**, 235106 (2020).
- [62] L. Feng, T. Shiga, and J. Shiomi, Phonon transport in perovskite SrTiO_3 from first principles, *Appl. Phys. Express* **8**, 071501 (2015).
- [63] A. I. Lebedev, *Ab initio* calculations of phonon spectra in ATiO_3 perovskite crystals ($A = \text{Ca}, \text{Sr}, \text{Ba}, \text{Ra}, \text{Cd}, \text{Zn}, \text{Mg}, \text{Ge}, \text{Sn}, \text{Pb}$), *Phys. Solid State* **51**, 362 (2009).
- [64] S. Petit, F. Damay, Q. Berrod, and J. M. Zanotti, Spin and lattice dynamics in the two-singlet system $\text{Tb}_3\text{Ga}_5\text{O}_{12}$, *Phys. Rev. Res.* **3**, 013030 (2021).
- [65] B. Fauqué, P. Bourges, A. Subedi, K. Behnia, B. Baptiste, B. Roessli, T. Fennell, S. Raymond, and P. Steffens, Mesoscopic fluctuating domains in strontium titanate, *Phys. Rev. B* **106**, L140301 (2022).
- [66] T. Katsufuji and Y. Tokura, Transport and magnetic properties of a ferromagnetic metal: $\text{Eu}_{1-x}\text{R}_x\text{TiO}_3$, *Phys. Rev. B* **60**, R15021 (1999).
- [67] C.-L. Chien, S. DeBenedetti, and F. D. S. Barros, Magnetic properties of EuTiO_3 , Eu_2TiO_4 , and $\text{Eu}_3\text{Ti}_2\text{O}_7$, *Phys. Rev. B* **10**, 3913 (1974).